Check for updates

JGR Space Physics

RESEARCH ARTICLE
10.1029/2021JA029115

Ground-Based Magnetometer Response to Impacting Magnetosheath Jets

L. Norenius[1], M. Hamrin[1], O. Goncharov[2], H. Gunell[1], H. Opgenoorth[1], T. Pitkänen[1,3], S. Chong[1], N. Partamies[4,5], and L. Baddeley[4,5]

[1]Department of Physics, Umeå University, Umeå, Sweden, [2]Faculty of Mathematics and Physics, Charles University, Prague, Czech Republic, [3]Space Physics and Astronomy Research Unit, University of Oulu, Oulu, Finland, [4]Department of Geophysics, The University Centre in Svalbard, Longyearbyen, Svalbard, Norway, [5]Birkeland Centre for Space Science, Bergen, Norway

Key Points:

- Ground-based magnetometers observe damped oscillations resulting from impacting jets
- The median damping time and observed frequency is 370 s and 1.9 mHz respectively
- We suggest that larger and more energetic jets might increase the amplitude of the ground-based magnetic response

Correspondence to:
L. Norenius,
linus.norenius@space.umu.se

Citation:
Norenius, L., Hamrin, M., Goncharov, O., Gunell, H., Opgenoorth, H., Pitkänen, T., et al. (2021). Ground-based magnetometer response to impacting magnetosheath jets. *Journal of Geophysical Research: Space Physics*, *126*, e2021JA029115. https://doi.org/10.1029/2021JA029115

Received 7 JAN 2021
Accepted 14 JUN 2021

Abstract Localized dynamic pressure pulses in the magnetosheath, or jets, have been a popular topic for discussion in recent decades. Studies show that they can propagate through the magnetosheath and impact the magnetopause, possibly showing up as geoeffective elements at ground level. However, questions still remain on how geoeffective they can be. Previous studies have been limited to case studies during few days and with only a handful of events. In this study we have found 65 cases of impacting jets using observations from the Multiscale Magnetospheric mission during 2015–2017. We examine their geoeffectiveness using ground-based magnetometers (GMAGs). From our statistics we find that GMAGs observe responses as fluctuations in the geomagnetic field with amplitudes of 34 nT, frequencies of 1.9 mHz, and damping times of 370 s. Further, the parallel length and the maximum dynamic pressure of the jet dictate the amplitude of the observed GMAG response. Longer and higher pressure jets inducing larger amplitude responses in GMAG horizontal components. The median time required for the signal to be detected by GMAGs is 190 s. We also examine if jets can be harmful for human infrastructure and cannot exclude that such events could exist.

1. Introduction

The terrestrial bow shock is a shock front formed in front of the magnetosphere where the supersonic solar wind abruptly decelerates to subsonic velocities. Downstream of the bow shock lies a turbulent region of warm dense plasma - the magnetosheath. In the magnetosheath, localized dynamic pressure enhancements are often observed examples (Amata et al., 2011; Archer et al., 2012; Karlsson et al., 2012). These pressure enhancements have been referred by many different names, for example, plasmoids (Gunell et al., 2012, 2014), antisunward high-speed jets (Plaschke et al., 2020), and supermagnetosonic subsolar magnetosheath jets (Hietala et al., 2012). In this article, we will refer to them as jets, or impacting jets.

Geoeffective jets, which are jets causing disturbances to the magnetosphere-ionosphere system, have raised attention. For instance, Hietala et al. (2012) investigated several jets measured during a period of one day by Cluster spacecraft. They compared the jet observations with simultaneous observations from the geostationary orbit by Geostationary Operational Environmental Satellite (GOES) and from the ionosphere by the Super Dual Aurora Network (SuperDARN) radars. Hietala et al. (2012) reported that during times with observations of jets, irregular pulsations in the magnetic field at the geostationary orbit could be seen. Furthermore, at the same time, localized enhanced ionospheric flows were observed by SuperDARN. Archer, Horbury, et al. (2013) performed a similar study using the Time History of Events and Macroscale Interactions during Substorms (THEMIS) spacecraft observations and ground-based magnetometer (GMAG) data as well as SuperDARN observations during a time period of 12 h. Also they could observe enhanced ionospheric flows associated with the periods with jet observations. Archer, Horbury, et al. (2013) characterized these flows as traveling convection vortices (TCVs, cf. (Glassmeier et al., 1989)). Further, Archer et al (2013) suggested that the magnetopause filters away pressure variations on timescales shorter than a few minutes, yielding a low-pass filter effect. Dmitriev and Suvorova (2012) conducted a case study for a single jet using THEMIS spacecraft observations and GMAG data. They reported that the magnetosheath jet in their event impacted the magnetopause causing it to distort in an "expansion-compression-expansion" sequence, which lasted for ~15 min. At the same time, the Chapman-Ferraro currents at the magnetopause were simi-

© 2021. The Authors.
This is an open access article under the terms of the Creative Commons Attribution-NonCommercial License, which permits use, distribution and reproduction in any medium, provided the original work is properly cited and is not used for commercial purposes.

larly distorted, which generated a magnetic pulse that could be seen as a "decrease-peak-decrease" sequence in the GMAG observations of the horizontal magnetic field component. Archer, Horbury et al. (2013) performed a statistical study using THEMIS and GOES observations suggesting that jets can drive magnetospheric ultralow frequency (ULF) waves at discrete frequencies.

The significance of magnetosheath jets in terms of geoeffectiveness is still unclear, and poses many questions. For instance, what is the time delay between jets and their potential ground-based signatures? How important are the jets for low-altitude magnetospheric and ionospheric variations? What is the signature of the ground-based response? Are only large jets able to induce a ground-based response? And what is their significance in terms of being disruptive for human infrastructure? In the space weather community, it is known that the so-called geomagnetically induced currents (GICs) can be harmful for infrastructure such as power lines (Boteler, 1994). How much can impacting jets affect infrastructure at ground level? Could these jets even create such GICs through strong dB/dt-effects?

We note that the data used in the studies mentioned above are limited in time, stretching over a few days and including only a handful of events at most. An exemption to this is the study by Archer, Horbury, et al. (2013) containing 130 events. However that study does not utilize simultaneous ground-based observations and stretches over a shorter time period. In this study, we perform a more extensive investigation using a larger data set stretching over a longer time. We examine jets impacting the magnetopause and their effects caused at ground level, as observed from GMAGs of the SuperMAG network (Gjerloev, 2009). The jets are identified from the Magnetosphere Multiscale (MMS) spacecraft (Burch & Phan, 2016) and the OMNI data (King & Papitashvili, 2005). We perform a case study of one selected event, and a statistical study of 65 similar events, where we compare the ground-based response to the jet plasma parameters. Based on the results, we then discuss and conclude with respect to the questions stated above.

2. Data and Event Selection

To select jets in the magnetosheath we use MMS and OMNI data. The four MMS spacecraft were launched in 2015 to monitor magnetic reconnetion in Earth's magnetosphere (Burch & Phan, 2016). They were launched in an elliptic equatorial orbit, with an apogee of 12 R_E and perigee of 1.2 R_E (geocentric distance) in the first phase of the mission. This provides a good coverage to monitor the dayside magnetosheath. We use data from the Fluxgate Magnetometer (FGM) which provides magnetic field measurements. We use fast survey mode data with 16-Hz sampling rate (Russell et al., 2014). In addition, we use the Fast Plasma Investigation (FPI) which provides plasma measurements with 4.5-s resolution in fast survey mode (Pollock et al., 2016). Note that we only use observations from MMS 1. To select the jets, we also use solar wind data propagated to the nominal bow shock. These data are provided by the NASA OMNIweb (King & Papitashvili, 2005). The OMNI data set consists of interplanetary magnetic field (IMF) and plasma observations with 4.5-s resolution.

SuperMAG (Gjerloev, 2009) is a world-spanning collaboration of organizations and institutes which gather and present ground-based magnetometer data (http://supermag.jhuapl.edu/). The data we use for this study are of 1-min time resolution. SuperMAG provides their data in a coordinate system decomposed into north, east, and vertically down components N, E, and Z, respectively (geographic, GEO coordinates). Furthermore, they provide the data with yearly and daily baselines removed (Gjerloev, 2012). We have restricted ourselves to only work with GMAG stations in the northern hemisphere, due to relative scarcity of stations in the southern hemisphere. Table 1 shows all GMAG stations used in this study, along with their IAGA (International Association of Geomagnetism and Aeronomy) code abbreviation and GEO coordinates.

In the literature there are many proposed criteria to select magnetosheath jets. In this study we use a slightly modified criteria from Archer and Horbury (2013). To select events for our statistical investigation, we select days when MMS is located in the magnetosheath by manually inspecting the ion energy-time spectrogram (i.e., Figure 1a). To increase the likelihood of any detected jets being on a collisional course with the magnetopause we also require that MMS is located within a 90° cone angle around the Sun-Earth line. Then we utilize our selection criterion based on the dynamic pressure, $P_d = m_p n v^2$ with the proton mass m_p, the plasma density n, and the bulk velocity v. The criterion requires that the total dynamic pressure surpasses two times the background value. This background value is obtained from a 20 min running average, $\langle P_d \rangle_{20\text{min}}$.

Table 1
List of GMAG Stations Used in This Article, With Names and Locations in GEO Coordinates

IAGA code	Name	Longitude [°]	Latitude [°]
NAL	Ny-Ålesund	12.35	79.32
BBG	Barentsburg	14.21	78.06
HRN	Hornsund	15.6	77
LYR	Longyearbyen	16.23	78.2
BJN	Bear Island	19.2	74.5
HOP	Hopen Island	25.01	76.51
NOR	Nordkapp	26.19	71.09
VIZ	Vieze Island	76.54	79.3
DIK	Dixon	80.7	73.53
TIK	Tixie	129.32	71.59
PBK	Pebek	170.9	70.08
THL	Qaanag	291.17	77.47
SVS	Savassivik	294.9	76.02
KUV	Kullorsuaq	303.22	74.57
UPN	Upernavik	304.25	73.18
GDH	Godhavn	306.47	69.25
DMH	Danmarkshavn	341.37	77.17
JAN	Jan Mayen	351.3	70.9

Abbreviations: GEO, geographic; GMAGs, ground-based magnetometers.

We also require that the plasma velocity is Earthward along the Sun-Earth line (negative in the x_{GSE}-direction) throughout the entire jet duration. We define the beginning of a jet as the instant when the dynamic pressure first exceeds $\langle P_d \rangle_{20\text{min}}$ and the end of the jet as the time when the dynamic pressure falls below that value again. In addition, if two jets are detected within one minute of each other, they are treated as a single jet regardless of whether the dynamic pressure decreases below $\langle P_d \rangle_{20\text{min}}$ in between the jets. To exclude possible bow shock crossings and solar wind plasma from our data set, we remove events where the plasma density and velocity reach those of the solar wind within 10% margins. These data are obtained from the OMNIweb (King & Papitashvili, 2005). This is manually inspected as well, comparing plasma velocities, Ion energy time spectrogram and magnetic field values from MMS to reduce the risk that any bow shock crossings are included.

Figure 1 shows an example event which will be discussed in more detail in Section 3.1. Panel e shows the dynamic pressure observations from MMS in the magnetosheath in black. It is defined as a jet since it exceeds two times the background value (blue). The yellow shading highlights the duration of the jet, that is, between the times it exceeds the background value (red). The duration can be used as a measure of the parallel length of the jet, l_p, assuming that the jet propagates at the observed ion velocity and that MMS probes close to the center of the jet (Goncharov et al., 2020). However, a recent study by Palmroth et al. (2021) indicates that estimating a jet's length scale from spacecraft observations can be misleading. For example, they found that the jets tend to get shorter as they progress through the magnetosheath. Hence these integrated length scales contains uncertainties. For the example event, the observed duration is ~5.5 min and integrating the velocity yields a $l_p \approx 10\ R_E$. Note that this is a very long duration jet. However, the choice to use this particular event as our example event is due to the relatively clear response in the GMAG observations which will be discussed further in Section 3.1.

For each detected jet in our database, we estimate which of these are likely to impact the magnetopause by propagating them in time steps of 1 s with their observed velocity (at the point of the maximum dynamic pressure) until they arrive at the nominal magnetopause given by the T96 Tsyganenko model (Tsyganenko, 1996). Upon reaching the first closed model field line, an impact is assumed to have taken place. From T96 we can then trace the affected field line and find an ionospheric foot-point.

GMAG stations within a radius of 2,000 km of the foot-point are selected for observations of the ground-based response to the detected jets. Superposing the data from the selected GMAG stations, for each event we form an envelope of the upper (U) and lower (L) bounds of the observed magnetic perturbation in nT, for each component B_N, B_E, and B_Z. The difference between the upper and lower bounds, ΔUL, are then calculated. This difference is used to quantify the ground-based response.

We estimate the shortest time t_{min} it will take for our observed magnetosheath jets to become detectable by GMAG stations. We assume that the jet propagates with its velocity through the magnetosheath in the time t_{MS}. Then a signal traveling as an Alfvén wave, an Alfvénic signal, during the time t_A. The signal travels along the affected field line from the model magnetopause at the Alfvén velocity, $v_a = \sqrt{B^2 / \mu_0 \rho}$ with B the magnetic field, μ_0 the permeability of vacuum and ρ the plasma mass density. Along the field line, we assume a constant proton plasma density down to 1 R_E altitude, where the density rapidly increases. Down to this altitude we use magnetic field values from the T96 model and a constant plasma density of $n = 2 \times 10^5\ \text{m}^{-3}$ (Gunell et al., 2014). In order to get a better estimate of the magnetospheric plasma density we would require observations inside the magnetosphere for each event (see for example Radoski and Carovillano (1966)) which we lack. The remaining time required to traverse the final distance from 1 R_E down to the ground level, is of the order of 10 s, see for example Lysak (1999). If we include these 10 s in t_A, we

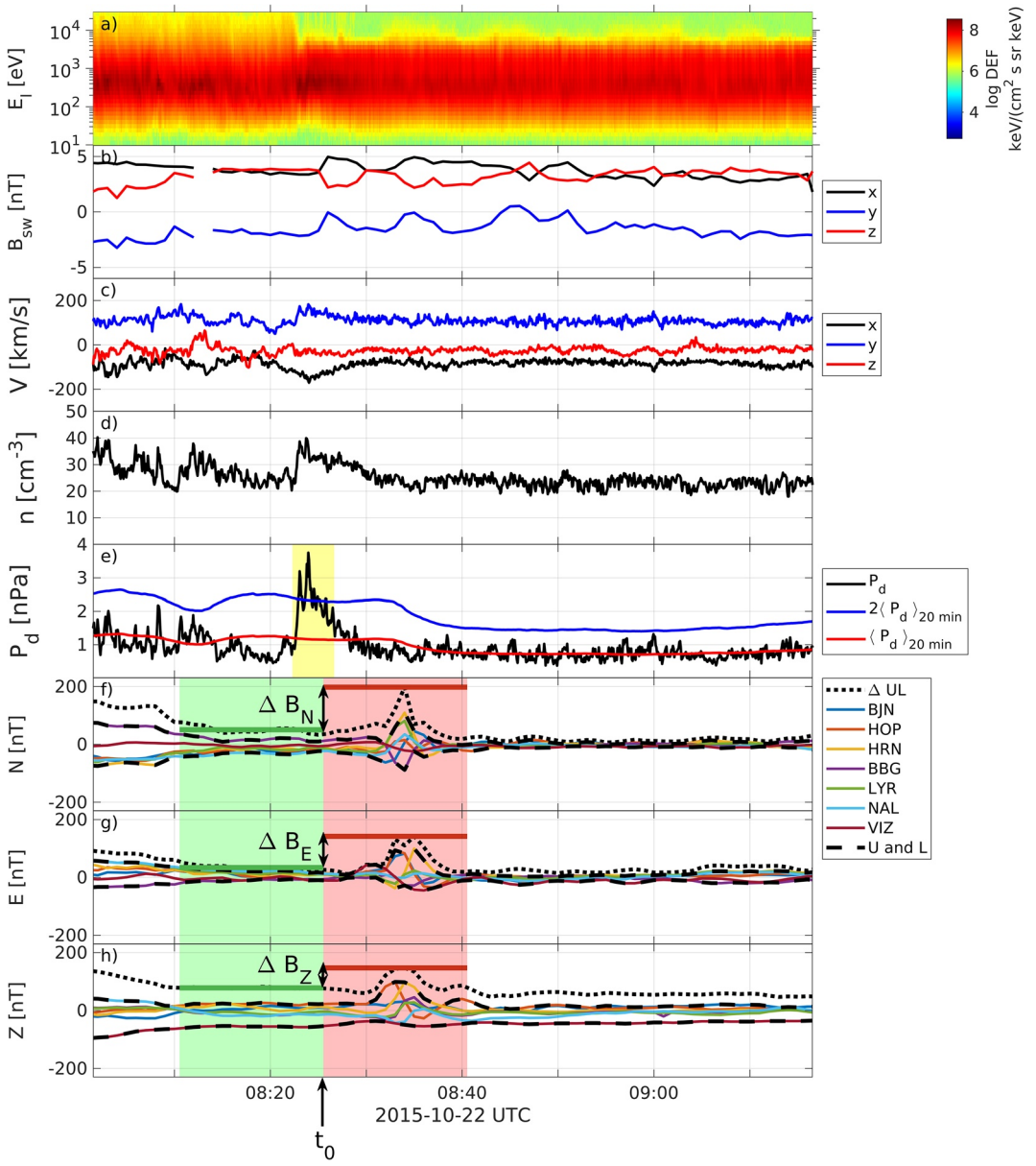

Figure 1. Selected event from 2015–10–22, (a) Ion energy-time spectrogram, (b) interplanetary magnetic field in geocentric solar ecliptic (GSE) coordinates from OMNI, propagated to the bow shock. (c) Ion velocity in GSE coordinates (d) and electron density as observed by Multiscale Magnetospheric (MMS). (e) Total dynamic pressure (black), two times the 20 min running average dynamic pressure $2\langle P_d \rangle_{20\text{min}}$ (blue), and the average $\langle P_d \rangle_{20\text{min}}$ (red) from MMS. (f–h) N, E, Z components of ground-based magnetometer observations. The green and red areas are used in calculating $\Delta B_{\text{N,E,Z}}$ (see the text for details).

find that $t_{\text{min}} = t_{\text{MS}} + t_A \approx 90$ s is the typical minimum time it takes before we can expect anything detectable at ground level. See also the discussion in Section 3.2. This estimated time can then be compared with the observed time. The observed time is defined as the time difference between when the center of the jet is observed by MMS to when an increase is observed it the GMAG observations. The increase criteria is defined as a 10% increase in any component.

To automatically quantify the ground-based response to a jet we assign a timestamp, t_0, 90 s after the peak of the jet. We then search for the maximum value of the ΔUL curve within a 15 min long interval after t_0. We compare this maximum with the mean of ΔUL during a 15 min interval preceding t_0 and we calculate the

difference between this maximum and mean. This defines $\Delta B_{N,E,Z}$ (for the respective components N, E, and Z) as the ground-based response possibly caused by the impacting jet.

Our data set of events are then finally also inspected manually. By looking at the standard deviation of the GMAG observations we discard cases when they are highly fluctuating possibly due to other reasons than jets. If the standard deviation during a 10 min window, 20 min before t_0 was larger than the standard deviation at a same size window just after t_0, they were considered highly fluctuating and discarded. We also require that the calculated foot-point captures at least three GMAG stations within 2,000 km. We have found 65 cases fulfilling the above mentioned criteria. We perform a statistical analysis of these cases, in terms of ground-based response.

3. Observations

3.1. Example Event

An example event measured on October 22, 2015, is shown in Figure 1. The top panel depicts the ion energy-time spectrogram from MMS. The spectrogram indicates that MMS was in the magnetosheath during the time, and that the upstream bow shock changed from quasi-parallel to quasi-perpendicular at around 08:22 UTC, as seen in the change of flux of high energy ions, see for example Raptis et al. (2020). We have also included IMF observations from OMNI in Figure 1b, propagated to the bow shock. The IMF is calm and steady between 08:10–08:22 UTC, but a discontinuity arrives around 08:22 UTC. This is likely the cause of the change from the quasi-parallel to quasi-perpendicular bow shock seen in the spectrogram. Panel c shows the observed ion velocity in GSE coordinates and panel d shows the electron density, both as observed by MMS. The next panel, e, shows total dynamic pressure in black as observed by MMS in the magnetosheath. The red (blue) line shows the background dynamic pressure (twice of the background value). During the time when the bow shock changed from quasi-parallel to quasi-perpendicular, there is an increase in the magnetosheath dynamic pressure, recorded as a jet. The jet starts at 08:22:30 UTC and ends at 08:28:10 UTC. The peak of this jet is at 08:24 UTC, and we assign t_0 at 08:25:30.

We estimate the theoretical time needed for this jet to be detectable at ground level according to our method described in Section 2. First, t_{MS} was estimated to be about 20 s. This number maybe underestimated since we assume that the jet propagates with its peak velocity at MMS position until it reaches the magnetopause. It is quite likely that the jet decelerates and changes direction as it moves through the magnetosheath, see for example Goncharov et al. (2020). Second, we estimate that the time required for an Alfvénic signal to reach 1 R_E altitude is $t_A \approx 40$ s. When adding the 10 s estimate for the travel time from 1 R_E to the ground, $t_A \approx 50$ s. This estimate is also associated with errors, mainly since we assume a constant density along the field line. Further, we only consider a proton plasma, while especially at lower altitudes other species play a role and lower the Alfvén velocity through heavier masses. In total, we estimate that the time required for any detectable response at ground level is $t_{min} = t_{MS} + t_A = 70$ s. We want to emphasize that this time is a minimum time required and we should probably expect to find a longer time between jet and ground-based response in the observations.

We estimate that the jet impacted the magnetopause at (9.2, 5.7, −0.6) R_E in GSE coordinates. We find the foot-point close to Svalbard, resulting in 7 GMAGs within 2,000 km and therefore being eligible for observations of the response. The N, E, and Z components of the magnetic field from these GMAGs are shown in Figures 1c–1e as solid colored lines. The upper and lower bounds of the envelope, U and L, are shown as black dashed lines, and lastly ΔUL as a black dotted line.

In Figures 1d–1f, we see how the GMAG observations are relatively steady before t_0 (green highlighted area). The variations around the mean (green solid line) is small as well. In the following 15 min (red highlighted area), we see a clear peak in ΔUL for all components about 10 min after t_0. Observable from the calculated $\Delta B_{N,E,Z}$, the N component shows a response of about 130 nT, slightly higher than the other two components. The E component response is about 100 nT and the Z component is the lowest, only showing a response of about 60 nT.

The VIZ station is the earliest one to observe any response to the jet and it is also the station closest to the predicted foot-point in this case, around 150 km north of the VIZ station and 1,300 km east of Svalbard.

The response starts at around 08:28 UTC, or 120 s after the center of the jet. This is 50 s longer than the estimated minimum time t_{min} for the jet to be detectable at ground level. In the E component, the response is quite clear while in the N and Z components it is less so. About one to two minutes after VIZ, HOP starts to show response in its N component, although lower in amplitude than VIZ. Eventually, the rest of the GMAGs display their observed response. But they start to do so at different times, with respect to the different stations and with respect to their individual components. One reason for this could be that the signal is traveling in the ionosphere, reaching GMAGs at different times. Another reason could be that the impact of the jet causes a signal with a larger spatial extent which travels and arrives at the ionosphere at different times. Archer, Horbury, et al. (2013) reported similar findings, where some stations observed a response earlier and other stations followed after. Worth noting is also the fact that the temporal resolution of the GMAG data is of only one minute. Compared to the estimated minimum time t_{min} the GMAG sampling time is relatively long, thus making it difficult to investigate the signal's ionospheric propagation based only on the GMAG timing.

Figures 1d–1f also shows that the response is in different directions among the stations. For example, BBG, BJN, and VIZ show a clear response in the negative N direction (southward magnetic disturbance) while most other stations show a positive response in their N component (northward disturbance). The same phenomena is seen in the E component as well: HRN, LYR, and NAL show a negative response (westward disturbance) at the start of their response and the other GMAGs show a positive response instead (eastward disturbance).

If we expect a radial disturbance of the magnetic field lines at the magnetopause due to an impacting magnetosheath jet, this should propagate as a polodial disturbance. Assuming no mode conversion at the ionosphere, then the wave should display as a north-south perturbation in the GMAG observations. However, Hughes (1974) suggested that such an Alfvénic wave must rotate 90° when it reaches the ionosphere, see also Sciffer et al. (2005), meaning a purely radial disturbance should be observed as an east-west perturbation at the GMAG observation. In our case the observation of the response indicates no clear north-south or east-west direction but something in between. Furthermore, since the jet impacted the magnetopause some distance away from the sub-solar point, we cannot assume that the disturbance is purely radial, and some azimuthal disturbance might be involved. Similarly, the predicted foot-point might be inaccurate to some degree, further diminishing a preferred direction of disturbance for the GMAGs.

It has been suggested that impacting magnetosheath jets might cause TCVs (Archer, Horbury, et al., 2013). Structures resembling TCVs have been recognized by Friis-Christensen et al. (1988) and Lanzerotti et al. (1986). They are generally considered to be traveling vortical flows in the ionosphere associated with field aligned currents (Murr et al., 2002). TCVs are commonly believed to be related to pressure variations in the solar wind (Amm et al., 2002). Hietala et al. (2012) found structures similar to TCVs although there was no evidence of any traveling of the observed ionospheric flow enhancements, thus are not entirely qualified as TCVs. The observations from our GMAGs show similar tendencies as those caused by TCVs. We have looked at the observed GMAG vectors over time for this case (not shown) and they resemble ones reported as being related to TCVs. However, this article is focused on the magnetic response to jets, not the ionospheric convection response so TCVs will not be discussed further.

Looking at the individual observations of the GMAGs, the responses seem to behave as damped oscillations. A large pulse is seen, followed by oscillations with a decreasing amplitude. For example, VIZ E component rises steadily by about 50 nT and then continues to oscillate with more damped peaks. The oscillations are less visible in the Z component, even though some stations show them there as well. It is the horizontal component that generally shows most activity. Therefore we only focus on the N and E components in the following.

To further study the damped oscillations we investigate the GMAG observations individually in more detail. We do this by applying curve-fitting, and analyzing the parameters resulting from the best fits. We perform the curve-fit for the N and E component of every GMAG. We then use the method proposed by Nelder and Mead (1965) for the numerical curve-fitting.

We chose the beginning of each curve-fit to be the point of the observation where the slope in the respective magnetic field component is the steepest. Each curve-fit is performed during a 30 min long window. To reduce

the error we first remove any linear trend from the data during this time window. Then we perform the fitting routine and select the events with low enough normalized root mean square (RMS) error for the study (more details as follows). The data is normalized by dividing it with the range of the data (max - min) from the specific time duration. The routine requires initial guesses of the parameters in $B(t) = A\exp(-t/\tau)\sin(f_{fit}t + \phi) + \epsilon$, with A the amplitude in nT, t the time and τ the e-folding time both in s, f_{fit} is the frequency, ϕ a phase shift and ϵ a offset. We chose the initial guesses for A by looking at the range of each observation, for f_{fit} by performing Fourier analysis of each observation, and for ϵ by using the mean of each observation. The two remaining parameters, τ and ϕ, are manually adjusted until the normalized RMS error is lower than 15%.

Figure 2 shows an example of our curve fitting results. The two columns represent the N and E components of each GMAG included for this event. The IAGA code of each station is presented for each row (see Table 1), these are all GMAGs within 2,000 km of the foot-point. We also show the normalized RMS error of the fit. The first harmonic frequency, f_{fit}, for each station and component is presented in each panel. All these plots were automatically generated, except HOP's N component since the automatic routine could not find a good fit. Instead, we manually added a second harmonic frequency, $f_2 = 2f$ to improve the fit. After this manual adjustment the RMS for HOP's N component became 14%. For this reason we chose 15% as the threshold, anything with a worse fit than HOP's N component shown here we decided to exclude. Apart from that particular GMAG station, the RMS error is low and the GMAG response can with a high accuracy be modeled as a damped harmonic oscillation. Averaging over all stations and components, we find that the observed mean frequency is around 2 mHz. Further, the e-folding time is found to be $\tau \sim 500$ s.

3.2. Statistical Study

The case we have shown in Figure 1 is typical among our data set, and we have found 65 similar ones (see Section 2). With these cases we can investigate the frequency observed by GMAGs and the time delay between impacting jets and ground-based response. We can also examine the amplitude of any observed ground-based response further, in terms of $\Delta B_{N,E,Z}$. In addition, in some of our cases we can perform curve fitting analysis. This allows us to further investigate the frequency and e-folding time, f_{fit} and τ respectively.

In order to get an estimate of the frequencies of the observed GMAG responses, we perform a simple Fourier analysis with Welch windowing on our 65 cases. We perform this analysis on all selected GMAGs and on both the N and E components separately and find the peak frequency in the spectra for each. Then we find the median of the N and E observations separately for each GMAG, and finally average this to get one frequency per jet. We start the Fourier transform 10 min before the observed jet and perform it over a 45 min long time window. The frequencies for each event are shown in Table 2 and the median frequency we find is 1.9 mHz. This is in good agreement with the reported magic ULF frequencies from Archer, Horbury, et al. (2013).

To further investigate the frequencies and damping times, we perform the curve fitting procedure described in Section 3.1 on more cases. We select cases where we can see clear damped oscillations among at least three of the GMAGs. Then we discard GMAG observations with RMS errors above 15%. This results in 10 cases being eligible. We find the median curve fit harmonic frequency as $f_{fit} \sim 1.7$ mHz. This is slightly lower than the median frequency observed through the simple Fourier analysis. However, comparing the Fourier frequency with the curve fit frequency case by case we find them to be in reasonable agreement, see Table 2.

When we looked at τ, the results we find are quite similar to the one presented in Figure 2. The relative spread of τ is however larger than what we observe for f_{fit}. The median value for we find as $\tau \sim 370$ s, meaning that after this median time, the effects from impacting jets would be considerably less visible among GMAG data. Dmitriev and Suvorova (2012) found one event using the THEMIS spacecraft where an impacting jet caused the magnetopause to move in an "expansion-compression-expansion" sequence which lasted for 15 min. This is slightly more than two times our found median value, thus it seems to be in good agreement with the result from Dmitriev and Suvorova (2012).

We can also try to crudely estimate which part of the jet that causes any geoeffective response. Is it enough for the leading edge of the jet to impact the magnetopause, or are larger parts of the jet required to cause measurable GMAG disturbances? We can answer this by assuming that the jet propagates through the

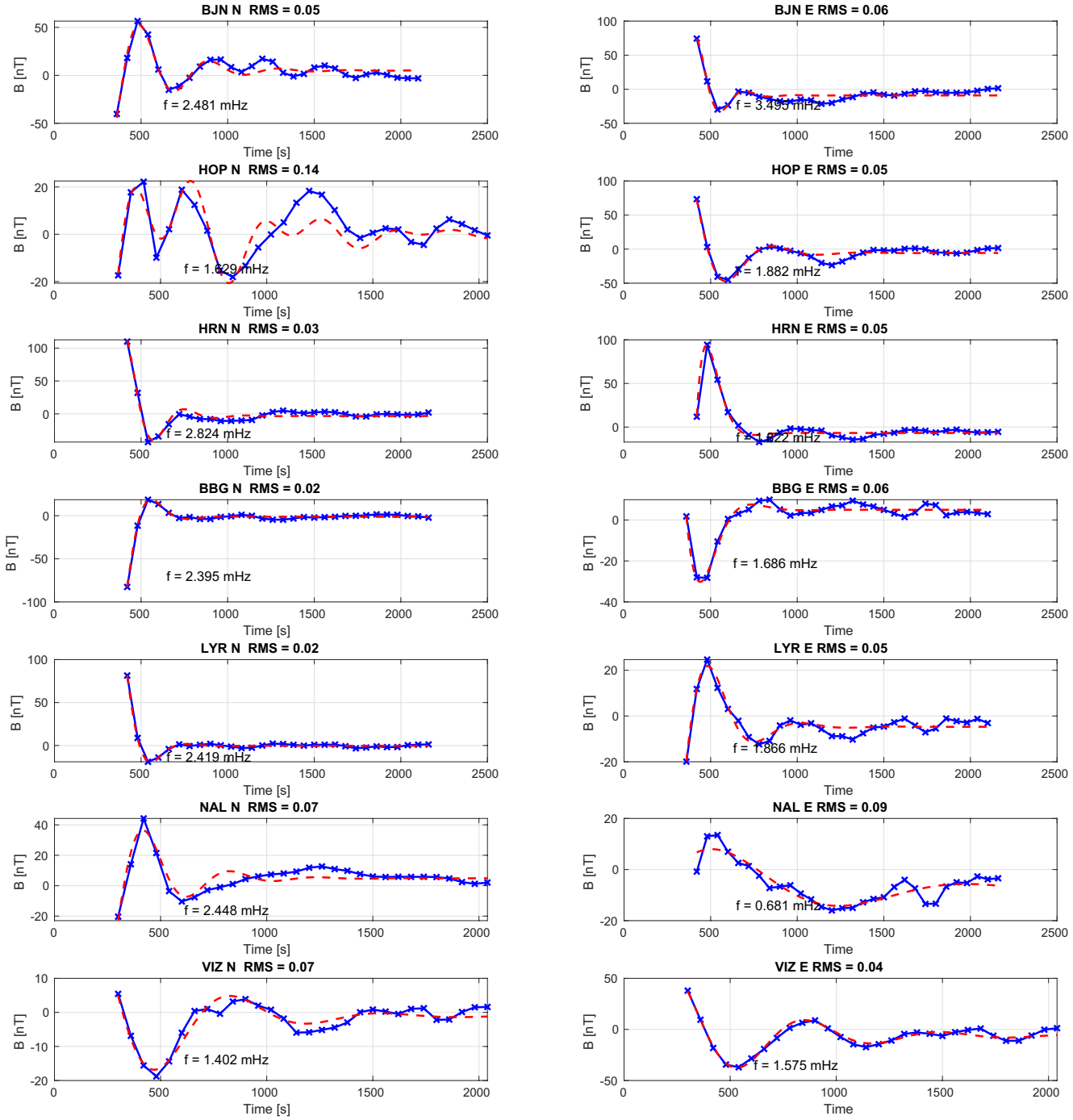

Figure 2. Shown in blue, ground-based magnetometer (GMAG) observation (any linear trend removed) from 2015–10–22 08:20–09:20 UTC from 7 GMAG stations close to the foot point at 91°, 79° latitude and longitude. Dashed red line shows best curve fit assuming a damped harmonic oscillation. Northward components are shown in the left column and eastward components in the right. The *x*-axis starts at 90 s after the maximum dynamic pressure of the jet. Root mean square error and frequencies are shown for each panel.

magnetosheath with its peak velocity, and then that an Alfvén signal is transmitted and propagates down into the ionosphere. Then we can compare our theoretically estimated times, $t_{\min} = t_{\mathrm{MS}} + t_A$ with our observed response times t. These times are also presented in Table 2. When measuring t, we measure from the center of the jet to the first visible response among the GMAGs. We can see that our estimated times are always shorter than the observed ones. In an attempt to reduce the discrepancy between these times we

Table 2
List of Events Included in Our Study.

Date and time yyyymmdd hh:mm	t_{MS} [s]	t_{AL} [s]	t_{min} [s]	t [s]	f [mHz]	f_{fit} [mHz]	τ [s]	Date and time yyyymmdd hh:mm	t_{MS} [s]	t_{AL} [s]	t_{min} [s]	t [s]	f [mHz]	f_{fit} [mHz]	τ [s]
20151020 09:01	50	66	116	140	1.5			20161213 09:35	7	80	87	181	2.7		
20151022 08:25	*29*	*66*	*95*	*234*	*1.9*	*2.0*	*488*	20161213 10:00	14	78	92	167	2.1		
20151023 08:42	*19*	*66*	*85*	*258*	*1.5*	*1.5*	*317*	20161213 10:20	12	77	89	323	2.2		
20151025 09:50	107	66	173	249	1.7			20161213 12:10	23	78	101	188	2.3		
20151113 06:30	0	72	72	184	1.8			20161214 06:50	0	66	66	146	2.2		
20151114 10:04	*120*	*72*	*192*	*234*	*2.2*	*1.8*	*217*	*20161215 09:15*	*14*	*80*	*94*	*100*	*2.2*	*1.3*	*760*
20151213 07:50	2	80	82	240	2.0			20161215 10:20	10	82	92	157	2.1		
20151224 05:19	72	44	116	170	1.9			20161216 10:50	27	90	117	229	1.6		
20151224 05:28	37	82	119	122	1.8			*20161216 12:10*	*11*	*78*	*89*	*367*	*1.9*	*1.4*	*645*
20160115 00:10	10	112	122	193	1.7			*20161223 06:00*	*5*	*55*	*60*	*187*	*2.0*		
20160121 04:21	46	63	109	176	3.0			20161224 04:10	0	53	53	179	1.8		
20160123 00:00	13	118	131	135	1.9			20161224 10:35	29	60	89	193	1.9		
20161106 12:40	47	79	126	167	1.9			20161225 06:40	16	57	73	272	2.1		
20161111 08:30	0	40	40	93	1.8			20161226 14:05	0	58	58	123	1.8		
20161112 16:00	19	84	103	204	2.0			20161227 08:10	9	73	82	311	2.4		
20161113 11:00	6	65	71	176	2.3			20161227 09:10	11	74	85	211	2.3		
20161120 07:45	*7*	*49*	*56*	*141*	*1.6*	*1.3*	*556*	20161229 09:00	23	66	89	241	1.9		
20161124 07:30	42	45	87	217	2.3			*20161230 09:30*	*30*	*65*	*95*	*378*	*2.1*	*2.0*	*641*
20161125 10:00	16	67	83	170	1.8			20170102 08:30	37	64	101	159	2.5		
20161126 09:05	4	72	76	246	1.8			20170104 11:35	22	52	74	235	2.1		
20161126 12:40	21	77	98	170	2.2			20170112 06:00	39	64	103	211	2.1		
20161126 15:40	*8*	*78*	*86*	*147*	*2.1*	*2.0*	*376*	20170112 06:20	54	68	122	141	1.8		
20161127 11:55	27	70	97	205	1.8			*0170112 06:50*	*48*	*68*	*116*	*205*	*1.8*	*2.0*	*531*
20161128 10:50	39	72	111	240	2.0			20170115 02:30	9	57	66	168	2.1		
20161202 09:55	10	87	97	217	1.6			20170115 04:35	35	61	96	169	2.2		
20161204 05:30	0	42	42	291	1.9			20170115 11:00	0	67	67	134	2.1		
20161204 08:00	0	69	69	198	2.3			20170117 08:20	60	57	117	334	1.9		
20161204 08:10	11	70	81	153	1.8			20170122 07:50	25	56	81	163	2.0		
20161204 08:50	25	71	96	189	1.7			20170123 03:10	0	72	72	176	3.9		
20161207 13:20	113	48	161	170	1.7			20170128 01:30	11	53	64	276	2.8		
20161210 05:05	0	45	45	131	1.8			20170130 01:50	12	62	74	155	1.5		
20161212 08:30	29	54	83	188	1.9			*20170130 02:00*	*23*	*63*	*86*	*188*	*1.6*	*1.0*	*350*
20161212 10:25	67	55	122	165	2.0										

Note.The times shown $t_{min} = t_{MS} + t_A$ are the estimated minimum time required for response, t_{MS} being the magnetosheath time and t_A the Alfvén time, and t being the observed times. The median of the observed frequencies of the GMAG responses are Listed as f. Each case included in the curve fitting analysis are listed in *italic*, together with its harmonic frequency and e-folding time f_{fit} and τ, respectively.

tried to add half the observed duration of the jets to t_{min}. When doing this, for some cases we see a better agreement between t_{min} and t, while for others the estimated times become longer than the observed ones (data not shown). Taking the median values of observed and estimated times, the comparison was in better agreement while doing this addition. This can tell us something about which part of the jet that actually transmits the Alfvén signal into the magnetosphere, which likely is somewhere between the middle and the trailing edge of the jet. It is however more difficult than this to find the geoeffective part of jets in reality.

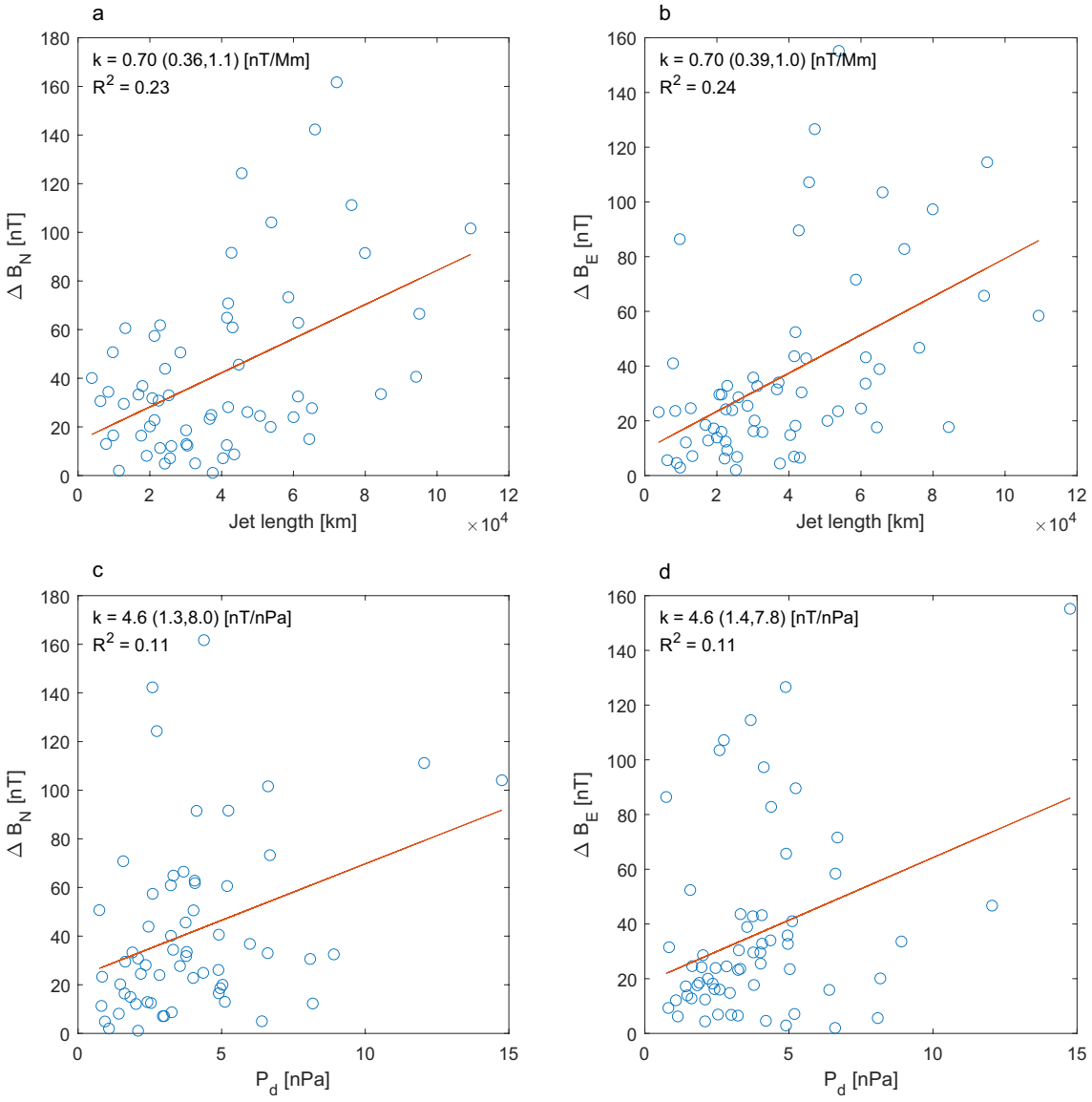

Figure 3. (a and b) show the calculated deviation from ground-based magnetometer observations in the N and E component respectively, in relation to observed jet parallel length. (c and d) show the deviation in the N and E component respectively in relation to the observed total dynamic pressure of the jets.

Since we lack magnetospheric density estimates for most of our cases this suggestion is based on a constant density. This is quite rough assumption and proper density observations would be required to further investigate this. Further, the shapes and morphology of jets found so far are inconsistent, see Section 4.3 in (Plaschke et al., 2018). Most size estimates assume a cylindrical geometry of jets, but it is probably likely that the shape is more irregular. Additionally, the observations indicate that the geoeffective part of the jets are different from jet to jet.

Our data set allows us to investigate some jet properties that are important for the amplitude of ground-based response in terms of ΔB. Using the method described in Section 2, and all our cases, we estimate the observed GMAG perturbation.

Figure 3 presents $\Delta B_{\mathrm{N,E}}$ as a function of the jet plasma parameters. The left and right column show the ground-based response observed in the N and E components, respectively. In panels a and b we show the response plotted against the parallel length of the jets, $l_p = \int v \mathrm{d}t$ during the observed duration t_{jet}. Panels c and d show the response versus the total dynamic pressure estimated at the peak of the jet with the background

pressure removed. For all panels, we have performed a linear fit as well, shown as a red solid line. The value of k (the slope) of each linear fit is shown in each panel with a 95% confidence interval, together with the R^2-value (the coefficient of determination). We can see that both the N and E component increases with the length of the jets. This seems reasonable, since larger jets should contain more energy and potentially yield a larger response. We examined the observed response as functions of the jets durations as well (not shown) where we saw similar trends although weaker with more scattering involved. The confidence interval contained negative numbers, however, the general trend of increasing response was still visible. Archer, Horbury, et al. (2013) presented a few cases with groups of jets with different durations, and concluded that the effects at ground level could only be seen when these groups exceeded a certain threshold duration of a couple of minutes. Thus the magnetopause would act as a low-pass filter. If one were to apply such a filter with a length much longer than the jets, the observed response would depend on the amount of power contained within the lower frequencies below the cut-off frequency of the filter. Depending on the jets amplitudes, this could typically generate a smooth decrease as the jets get shorter. This is matching with our observations. As such, our observations could be in agreement with the low-pass filtering effect suggested by Archer, Horbury, et al. (2013).

Considering the total dynamic pressure (Figures 3c and 3d), there is an increasing trend in the response as the pressure gets higher. Since dynamic pressure corresponds to kinetic energy density, it does not seem unreasonable to expect this increasing trend. More energetic jets would probably have a larger impact on the magnetosphere. One could suggest to not treat timescales and dynamic pressure separately, but rather see them combined. To do this, we looked at the integrated dynamic pressure (data not shown), a measure of energy content per jet. The general trend of increasing response remained and did not present any new conclusions.

Comparing panels a-b with c-d it would seem that the lengths of the jets might be more important than dynamic pressure when it comes to generating observable ground-based response. This is visible the larger R^2-values. However, due to the small values of R^2 it might be difficult to draw any real conclusion based solely on that. There is also a bias toward shorter and lower pressure jets in our data set which might skew the results as well. The trends look quite weak from a statistical point of view, but they are nonetheless increasing. Even if the correlation between length and dynamic pressure with GMAG response is not linear, there certainly seems to be an increased observed response as these quantities gets larger. Lastly, from all these cases, we find that the average of the observed ΔB is around 34 nT, with a standard deviation of a similar value. However, our highest observed ΔB was found as ~160 nT. Thus the range of the observed responses are quite large.

4. Summary and Discussion

In this study we have examined the effects of magnetosheath jets impacting the dayside magnetopause, as seen from GMAGs. The jets were detected in the magnetosheath using MMS and OMNI observations. Assuming that the jets travel at their observed plasma velocity we estimate their foot point by utilizing the T96 model. The timing of the jets, from detection by MMS to any observable GMAG response, we estimate with the jets plasma velocity and the distance to the nominal magnetopause from T96, together with the estimated Alfvén velocity through the magnetosphere. Magnetic field values was taken from T96 and we used a constant plasma density for determining the Alfvén velocity. This is a Our example event presented in Figure 1 shows that some GMAGs observe ground-based response as damped oscillations, especially in the N and E components, see Figure 2. We can also see that the amplitude of the response is different in different directions. Although this is beyond the scope of this article, it would be interesting to examine this in more detail. In this case, the estimated time is shorter than the observed time between the jet detection and the GMAG response, ~70 s compared to the observed ~120 s.

We have found 65 cases with observable perturbations in the low altitude magnetic field. We suggest that they are, due to their localizations and timings compared to estimated foot points and times, likely to be caused by impacting jets. We find that the time delay between the center of a detected jet and the start of the observed ground-based response is about 190 s (median). This is consistent with our assumptions that the jet travels in the magnetosheath with its observed velocity during peak dynamic pressure. Followed

by an Alfvénic signal traveling along the magnetic field line into the ionosphere upon impact with the magnetopause. Our estimated median time delay is 90 s, out of which a median of ∼56 s is required for the Alfvén signal to propagate from the magnetopause down to the ground. Using these results, together with observations of each jet's duration, and assuming a constant magnetospheric plasma density, we can try to estimate which part of the jet that carries the geoeffectiveness. This way we estimate that the Alfvénic signal is transmitted only after a majority of the jet's extent has reached the magnetosphere. However, this suggestion is dependent on our assumed constant plasma density and on the position of the magnetopause estimated by the T96 model. The density is known to vary significantly in the magnetosphere which alters the Alfvén velocity. And the T96 produced magnetopause can be quite far away from the real one, affecting t_{MS}. Hence this conclusion cannot be certain without magnetospheric observations of the density for all of our events. A study with better estimates of the magnetospheric density would be helpful to further increase the knowledge of how geoeffective jets affect us at ground level.

For all our cases, we observe that the GMAG response to an impacting jet contains some sort of oscillations. For a select number of cases, they resemble damped harmonic oscillations rather well. We have estimated the frequency, f, and the e-folding time, τ, of these oscillations using both Fourier analysis and curve fittings. We find that $f \sim 1.9$ mHz and $\tau \sim 370$ s. This is consistent with Pc5 waves whose amplitude are damped by $1/e$ within one wave period. Waves of similar frequencies, Pc5-range (1.6–7 mHz), have been reported as a result of impacting jets by Archer, Horbury, et al. (2013), although at much higher altitudes. ULF waves within this frequency range have been examined previously, by for example (Lysak et al., 1994) and (Hudson et al., 2004). They are thought to play an important role in the mass and energy transport in the magnetosphere (Allan et al., 1990; Elkington et al., 1999; Lotko et al., 1998). The observed average amplitude of all our observed ΔB is ∼34 nT, but with a rather large range.

We have also examined jet properties that are important for geoeffective responses. We found that the duration and peak dynamic pressure are two important properties of the jets in this regard. Assuming that the jet propagates along the observed velocity, the duration would correspond to the jet's spatial extent along this direction, while the dynamic pressure corresponds to kinetic energy density. Under this assumption, we found that larger and more energetic jets should be more geoeffective, see Figure 3. This could perhaps be expected since one would probably expect a larger jet to have higher dynamic pressure. However, in our data set we could not conclude this.

Worth noting is that in some of our cases, the bow shock changes from quasi-parallel to quasi-perpendicular at the time of jet observations by MMS, events similar to those listed as boundary jets by Raptis et al. (2020). This can be related to changes in the IMF that might go unnoticed in the OMNI observations. Hence, some of our observed GMAG responses might be related to such changes in the IMF, causing the foreshock to change. Though it is still possible that the jets play a role as well in causing the observed responses.

Archer, Horbury, et al. (2013) used single-day THEMIS observations to examine a handful of impacting jets and the effects caused by them inside the magnetosphere and at ground level. They reported that the magnetopause filters away pressure variations shorter than a few minutes, yielding a low-pass filter effect. Due to the impulsive structure of jets they are necessarily broadband and the contained power are carried over a large range of frequencies. Applying a low-pass filter will typically yield a smooth decrease of the output, which are consistent with our observations.

We should not that in this study we have treated all of our jets the same. That is, we have made no distinction of different types of jets which could differ due to their creations. Nor have we considered the complicated morphology of the jets as they traverse the magnetosheath. Palmroth et al. (2021) recently performed a study where they via simulations investigated the evolution of jets. Goncharov et al. (2020) also investigated this evolution. It would be interesting to redo our study but taking into consideration how the jets decelerate through the magnetosheath. This could maybe clarify the bias toward shorter/low dynamic pressure jets seen in Figure 3. Similarly, the different categories of jets listed by Raptis et al. (2020) could also be included in such a study.

Lastly, we note that the geomagnetic fields, which we observe at ground-level, are clearly perturbed in response to each of the inferred magnetosheath jets. We know that perturbations of this sort that are strong and fast enough (high dB/dt) could be harmful for infrastructure such as power lines through geomagnetically

induced currents, GICs (Boteler et al., 1998). Among our cases, the largest perturbation observed by GMAGs we saw was ~158 nT (Figure 3). Assuming that all impacting jets induce ground-based signals with around 2 mHz frequency, this would mean that it would take around 4 min for the signal to oscillate between its maximum and minimum value. This results in an average dB/dt ~40 nT/min, which is likely not that harmful for infrastructure. According to Kappenman (2006), power grid impacts of importance have been reported at levels even lower than 100 nT/min. If we assume that the linear trend depicted in Figure 3d continues toward larger dynamic pressures, assuming $n = 44\ cm^{-3}$ (median density for all our jets), we can estimate that jets reaching velocities of ~550 km/s could lead to $dB/dt \approx 100$ nT/min. Although this velocity can be considered high for jets, they have been reported reaching almost 500 km/s (Plaschke et al., 2013). However, since the magnetopause maps to the polar region with major infrastructure being quite sparse, the actual impact of magnetosheath jets and their harmfulness is probably very low regarding infrastructure.

Data Availability Statement

We thank the MMS Science Data Center and all the MMS teams, especially the magnetic field and the ion teams, for producing high-quality data avaliable at https://lasp.colorado.edu/mms/sdc/public/. We acknowledge use of NASA/GSFC's Space Physics Data Facility's OMNIWeb service, and OMNI data avaliable at https://omniweb.gsfc.nasa.gov/. We also acknowledge use of SuperMAG data which can be found at http://supermag.jhuapl.edu/mag/.

Acknowledgments
L. Norenius and M. Hamrin was supported by Vetenskapsrådet (VR) dnr 2018–03623. T. Pitkänen was supported by the Swedish National Space Agency (SNSA) grant 118/17. O. Goncharov was supported by the Kempe Foundation. H. Gunell was supported by the Swedish National Space Agency (SNSA) grant 108/18.

References

Allan, W., Manuel, J. R., & Poulter, E. M. (1990). Does the ponderomotive force move mass in the magnetosphere? *Geophysical Research Letters*, *17*(7), 917–920. https://doi.org/10.1029/GL017i007p00917

Amata, E., Savin, S., Ambrosino, D., Bogdanova, Y., Marcucci, M., Romanov, S., & Skalsky, A. (2011). High kinetic energy density jets in the earth's magnetosheath: A case study. *Planetary and Space Science*, *59*(7), 482–494. https://doi.org/10.1016/j.pss.2010.07.021

Amm, O., Engebretson, M., Hughes, T., Newitt, L., Viljanen, A., & Watermann, J. (2002). A traveling convection vortex event study: Instantaneous ionospheric equivalent currents, estimation of field-aligned currents, and the role of induced currents. *Journal of Geophysical Research*, *107*, 1334. https://doi.org/10.1029/2002JA009472

Archer, M. O., Hartinger, M. D., & Horbury, T. S. (2013). Magnetospheric "magic" frequencies as magnetopause surface eigenmodes. *Geophysical Research Letters*, *40*(19), 5003–5008. https://doi.org/10.1002/grl.50979

Archer, M. O., Horbury, T., & Eastwood, J. (2012). Magnetosheath pressure pulses: Generation downstream of the bow shock from solar wind discontinuities. *Journal of Geophysical Research*, *117*, A05228. https://doi.org/10.1029/2011JA017468

Archer, M. O., & Horbury, T. S. (2013). Magnetosheath dynamic pressure enhancements: Occurrence and typical properties. *Annales Geophysicae*, *31*(2), 319–331. https://doi.org/10.5194/angeo-31-319-2013

Archer, M. O., Horbury, T. S., Eastwood, J. P., Weygand, J. M., & Yeoman, T. K. (2013). Magnetospheric response to magnetosheath pressure pulses: A low-pass filter effect. *Journal of Geophysical Research: Space Physics*, *118*(9), 5454–5466. https://doi.org/10.1002/jgra.50519

Boteler, D., Pirjola, R., & Nevanlinna, H. (1998). The effects of geomagnetic disturbances on electrical systems at the earth's surface. *Advances in Space Research*, *22*(1), 17–27. https://doi.org/10.1016/S0273-1177(97)01096-X

Boteler, D. H. (1994). Geomagnetically induced currents: Present knowledge and future research. *IEEE Transactions on Power Delivery*, *9*(1), 50–58. https://doi.org/10.1109/61.277679

Burch, J. L., & Phan, T. D. (2016). Magnetic reconnection at the dayside magnetopause: Advances with mms. *Geophysical Research Letters*, *43*(16), 8327–8338. https://doi.org/10.1002/2016GL069787

Dmitriev, A. V., & Suvorova, A. V. (2012). Traveling magnetopause distortion related to a large-scale magnetosheath plasma jet: Themis and ground-based observations. *Journal of Geophysical Research*, *117*(A8), 16. https://doi.org/10.1029/2011JA016861

Elkington, S. R., Hudson, M. K., & Chan, A. A. (1999). Acceleration of relativistic electrons via drift-resonant interaction with toroidal-mode pc-5 ulf oscillations. *Geophysical Research Letters*, *26*(21), 3273–3276. https://doi.org/10.1029/1999GL003659

Friis-Christensen, E., McHenry, M. A., Clauer, C. R., & Vennerstrøm, S. (1988). Ionospheric traveling convection vortices observed near the polar cleft: A triggered response to sudden changes in the solar wind. *Geophysical Research Letters*, *15*(3), 253–256. https://doi.org/10.1029/gl015i003p00253

Gjerloev, J. W. (2009). A global ground-based magnetometer initiative. *Eos Transactions - American Geophysical Union*, *90*(27), 230–231. https://doi.org/10.1029/2009EO270002

Gjerloev, J. W. (2012). The supermag data processing technique. *Journal of Geophysical Research*, *117*(A9), A09213. https://doi.org/10.1029/2012JA017683

Glassmeier, K.-H., Hönisch, M., & Untiedt, J. (1989). Ground-based and satellite observations of traveling magnetospheric convection twin vortices. *Journal of Geophysical Research*, *94*(A3), 2520–2528. https://doi.org/10.1029/JA094iA03p02520

Goncharov, O., Gunell, H., Hamrin, M., & Chong, S. (2020). Evolution of high-speed jets and plasmoids downstream of the quasi-perpendicular bow shock. *Journal of Geophysical Research: Space Physics*, *125*(6), e2019JA027667. https://doi.org/10.1029/2019JA027667

Gunell, H., Nilsson, H., Stenberg, G., Hamrin, M., Karlsson, T., Maggiolo, R., et al. (2012). Plasma penetration of the dayside magnetopause. *Physics of Plasmas*, *19*(7), 072906. https://doi.org/10.1063/1.4739446

Gunell, H., Stenberg Wieser, G., Mella, M., Maggiolo, R., Nilsson, H., Darrouzet, F., et al. (2014). Waves in high-speed plasmoids in the magnetosheath and at the magnetopause. *Annales Geophysicae*, *32*(8), 991–1009. https://doi.org/10.5194/angeo-32-991-2014

Hietala, N., Laitinen, T., Clausen, L., Facskó, G., Vaivads, A., Lucek, E., et al. (2012). Supermagnetosonic subsolar magnetosheath jets and their effects: From the solar wind to the ionospheric convection. *Annales Geophysicae*, *30*, 33–48. https://doi.org/10.5194/angeo-30-33-2012

Hudson, M. K., Denton, R. E., Lessard, M. R., Miftakhova, E. G., & Anderson, R. R. (2004). A study of pc-5 ulf oscillations. *Annales Geophysicae*, *22*(1), 289–302. https://doi.org/10.5194/angeo-22-289-2004

Hughes, W. (1974). The effect of the atmosphere and ionosphere on long period magnetospheric micropulsations. *Planetary and Space Science*, *22*(8), 1157–1172. https://doi.org/10.1016/0032-0633(74)90001-4

Kappenman, J. G. (2006). Great geomagnetic storms and extreme impulsive geomagnetic field disturbance events—An analysis of observational evidence including the great storm of May 1921. *Advances in Space Research*, *38*(2), 188–199. https://doi.org/10.1016/j.asr.2005.08.055

Karlsson, T., Brenning, N., Nilsson, H., Trotignon, J.-G., Vallières, X., & Facsko, G. (2012). Localized density enhancements in the magnetosheath: Three-dimensional morphology and possible importance for impulsive penetration. *Journal of Geophysical Research*, *117*(A3), A03227. https://doi.org/10.1029/2011JA017059

King, J. H., & Papitashvili, N. E. (2005). Solar wind spatial scales in and comparisons of hourly wind and ace plasma and magnetic field data. *Journal of Geophysical Research*, *110*(A2), A02104. https://doi.org/10.1029/2004JA010649

Lanzerotti, L. J., Lee, L. C., Maclennan, C. G., Wolfe, A., & Medford, L. V. (1986). Possible evidence of flux transfer events in the polar ionosphere. *Geophysical Research Letters*, *13*(11), 1089–1092. https://doi.org/10.1029/GL013i011p01089

Lotko, W., Streltsov, A. V., & Carlson, C. W. (1998). Discrete auroral arc, electrostatic shock and suprathermal electrons powered by dispersive, anomalously resistive field line resonance. *Geophysical Research Letters*, *25*(24), 4449–4452. https://doi.org/10.1029/1998GL900200

Lysak, R. L. (1999). Propagation of Alfvén waves through the ionosphere: Dependence on ionospheric parameters. *Journal of Geophysical Research*, *104*(A5), 10017–10030. https://doi.org/10.1029/1999ja900024

Lysak, R. L., Song, Y., & Lee, D.-H. (1994). Generation of ULF waves by fluctuations in the magnetopause position. *Washington DC American Geophysical Union Geophysical Monograph Series*, *81*, 273–281. https://doi.org/10.1029/GM081p0273

Murr, D. L., Hughes, W. J., Rodger, A. S., Zesta, E., Frey, H. U., & Weatherwax, A. T. (2002). Conjugate observations of traveling convection vortices: The field-aligned current system. *Journal of Geophysical Research: Space Physics*, *107*, 1306. https://doi.org/10.1029/2002JA009456

Nelder, J. A., & Mead, R. (1965). A simplex method for function minimization. *The Computer Journal*, *7*(4), 308–313. https://doi.org/10.1093/comjnl/7.4.308

Palmroth, M., Raptis, S., Suni, J., Karlsson, T., Turc, L., Johlander, A., et al. (2021). Magnetosheath jet evolution as a function of lifetime: Global hybrid-vlasov simulations compared to mms observations. *Annales Geophysicae*, *39*(2), 289–308. https://doi.org/10.5194/angeo-39-289-2021

Plaschke, F., Hietala, H., & Angelopoulos, V. (2013). Anti-sunward high-speed jets in the subsolar magnetosheath. *Annales Geophysicae*, *31*(10), 1877–1889. https://doi.org/10.5194/angeo-31-1877-2013

Plaschke, F., Hietala, H., & Vörös, Z. (2020). Scale sizes of magnetosheath jets. *Journal of Geophysical Research: Space Physics*, *125*(9), e2020JA027962. https://doi.org/10.1029/2020JA027962

Plaschke, F., Hietala, M., Blanco-Cano, X., Kajdič, P., Karlsson, T., Sibeck, D., et al. (2018). Jets downstream of collisionless shocks. *Space Science Reviews*, *214*(5), 81. https://doi.org/10.1007/s11214-018-0516-3

Pollock, C., Moore, T., Jacques, A., Burch, J., Gliese, U., Saito, Y., et al. (2016). Fast plasma investigation for magnetospheric multiscale. *Space Science Reviews*, *199*(1–4), 331–406. https://doi.org/10.1007/s11214-016-0245-4

Radoski, H. R., & Carovillano, R. L. (1966). Axisymmetric plasmasphere resonances: Toroidal mode. *Physics of Fluids*, *9*(2), 285–291. https://doi.org/10.1063/1.1761671

Raptis, S., Karlsson, T., Plaschke, F., Kullen, A., & Lindqvist, P.-A. (2020). Classifying magnetosheath jets using mms: Statistical properties. *Journal of Geophysical Research: Space Physics*, *125*(11), e2019JA027754. https://doi.org/10.1029/2019JA027754

Russell, C. T., Anderson, B. J., Baumjohann, W., Bromund, K. R., Dearborn, D., Fischer, D., et al. (2014). The magnetospheric multiscale magnetometers. *Space Science Reviews*, *199*(1–4), 189–256. https://doi.org/10.1007/s11214-014-0057-3

Sciffer, M. D., Waters, C. L., & Menk, F. W. (2005). A numerical model to investigate the polarisation azimuth of ulf waves through an ionosphere with oblique magnetic fields. *Annales Geophysicae*, *23*(11), 3457–3471. https://doi.org/10.5194/angeo-23-3457-2005

Tsyganenko, N. A. (1996). Effects of the solar wind conditions in the global magnetospheric configurations as deduced from data-based field models (Invited). In E. J. Rolfe, & B. Kaldeich (Eds.), *International conference on substorms* (Vol. 389, p. 181).